This is the author's version of an article that has been published in this journal. Changes were made to this version by the publisher prior to publication. The final version is available at https://dx.doi.org/10.1109/TMTT.2025.3588177

Space Mapping with Parameter Extraction Based on the Kullback-Leibler Distance Illustrated with Full-Wave EM and Equivalent Circuit Models for Microstrip Filters

Roberto Loera-Díaz and José E. Rayas-Sánchez

Abstract—**Space mapping (SM) techniques are commonly used for optimizing highly accurate models that require a large computational effort, known as fine models, by exploiting simplified physics-based models that are computationally fast but not accurate enough, known as coarse models. Most SM formulations require solving a parameter extraction (PE) sub-problem at each iteration. Typically, SM algorithms use classical *l*-th norms for the PE objective function. In this paper, we first apply a PE formulation based on the Kullback-Leibler (K-L) distance to microstrip filters using their full-wave electromagnetic (EM) responses as targets, performing a rigorous numerical comparison against PE using classical norms. We subsequently propose, for the first time, a Broyden-based input space mapping algorithm using the K-L distance as objective function for the PE sub-problem. We apply SM design optimization to several examples, beginning with a classical synthetic test example and following with some microstrip filters using their full-wave EM representation as fine models, and their equivalent distributed circuit as coarse models. A rigorous numerical comparison is also performed between classical *l*-th norms and the K-L formulation for PE within the corresponding SM design optimizations. Our results indicate that SM with PE using the K-L formulation outperforms that one obtained by using the classical *l*-th norm PE formulations within SM.**

Index Terms—**Broyden, Chebyshev, EM, Euclidean, filter, Kullback-Leibler, Manhattan, microstrip, norm, optimization, parameter extraction, space mapping.**

I. Introduction

Space mapping (SM) techniques are used for the optimization of engineering models that are highly accurate but computationally expensive, named as fine models, with the support of physics-based auxiliary models that are fast but insufficiently accurate, named as coarse models [1], [2], [3]. Many space mapping algorithms [4], [5] require solving a parameter extraction (PE) sub-problem at each SM iteration [6], [7], which consists of finding the coarse model parameters that make the coarse model response as close as possible to the fine model response at the current iterate. This PE sub-problem has a very important impact on the stability and convergence of space mapping algorithms [4],[5],[7],[8]. Objective functions based on classical norms, also referred as *l*-th norms, have been traditionally employed to do PE [9].

A very recent development for PE in the context of SM consists of translating conventional microwave responses (e.g., $|S_{21}|$ evaluated over a broad frequency sweep) into a few problem-dependent key features based on engineering experience [10]. This approach has been recently adapted to formulate a cognitive SM technique [11]. However, in this paper, we focus on the effects of applying different PE formulations on conventional microwave responses directly generated by commercially available high-frequency simulators.

On a totally different context, in the field of information theory, the Kullback-Leibler (K-L) distance formulation was developed [12] as an approach inspired in Shannon entropy theory for measuring the "distance" or "divergence" in statistical populations. This formulation resulted in an efficient technique for measuring the difference between two probability distributions. It has been used in different fields and applications, *e.g.*, in speech synthesis to measure spectral distances [13], in image processing for texture retrieval [14], and in gas sensors for odor discrimination [15], among others. As confirmed in Section III of this paper, the K-L formulation resulted in a very suitable objective function to extract the parameters of a circuital model to match a typical RF or microwave response used as a target, given its larger dynamic range and smoother contours, as demonstrated in [16].

An experimental formulation for PE in the context of SM was proposed in [16] by exploiting the K-L distance to measure the local alignment between coarse and "fine" model responses, demonstrating a promising behavior of the resultant PE objective functions in some 1- and 2-dimensional synthetic examples [16]. It was observed that K-L formulations produce smoother PE objective functions with larger dynamic ranges as compared to those produced with classical *l*-th norms [16].

This paper corresponds to a substantial expansion of our work in [17], where we first use the K-L distance formulation for PE, as defined in [16], and apply it to microstrip filters whose target response is obtained from an accurate full-wave EM simulation, while the corresponding model responses are

This paper is an expanded version from the 2025 IEEE MTT-S Latin America Microwave Conference (LAMC), San Juan, Puerto Rico, Jan. 22-24, 2025.

R. Loera-Díaz and J. E. Rayas-Sánchez are with the Department of Electronics, Systems, and Informatics, ITESO – The Jesuit University of Guadalajara, Tlaquepaque, Jalisco, 45604 Mexico (e-mail: ng720156@iteso.mx; erayas@iteso.mx). R. Loera-Díaz was funded through a CONACYT scholarship (*Consejo Nacional de Ciencia y Tecnología,* Mexican Government). R. Loera-Díaz is also with Continental Automotive Group, Tlaquepaque, Jalisco, 45601 Mexico.

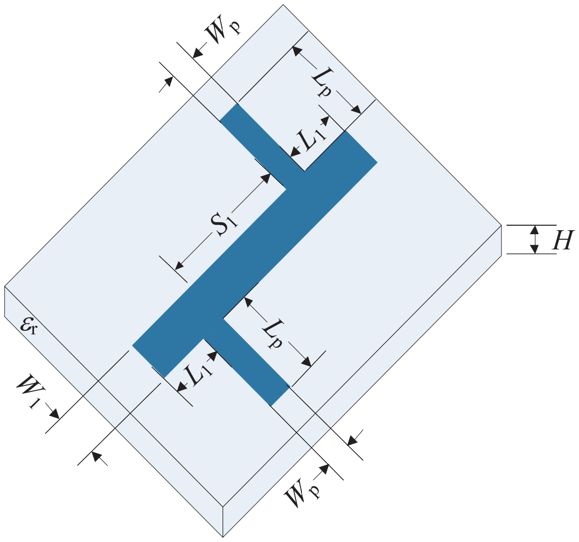

Fig. 1 Low-pass filter in microstrip technology [20]. The design parameters are $\boldsymbol{x} = [W_1 \quad L_1 \quad S_1]^{\mathrm{T}}$. From [17].

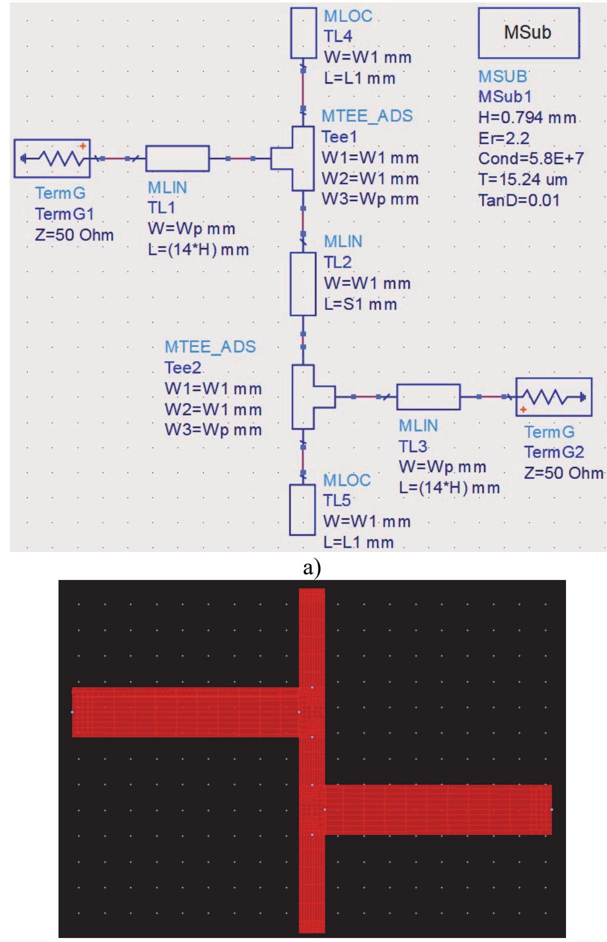

Fig. 2 Low-pass filter in microstrip technology: a) coarse model in ADS, b) fine model in ADS Momentum. From [17].

fast equivalent circuits in Keysight ADS [17]. A rigorous numerical comparison of PE using the K-L formulation against PE using classical norms (Manhattan, Euclidean, and Chebyshev) is performed, confirming the advantages found in [16]. In this expanded version of our work in [17], we provide essential background on SM and make explicit the stopping criteria used in our SM examples for rigorous comparisons. We next propose, for the first time, a Broyden-based input SM algorithm [7] that applies the K-L distance formulation in the PE sub-problem at each SM iteration. The proposed SM algorithm with K-L distance for PE is first applied to a classical synthetic example and then to several microstrip filters whose fine models use accurate full-wave EM models and the corresponding coarse models are equivalent circuits in Keysight ADS. We also perform a rigorous numerical comparison of this SM algorithm with PE using the K-L formulation against SM with classical norms for PE. We show that the proposed SM with K-L formulation for PE numerically outperforms the corresponding SM with classical l-th norms for the PE sub-problem.

The rest of the paper is organized as follows. Section II revisits PE objective functions and reintroduces the Kullback-Leibler distance for PE. Section III compares PE with classical l-th norms against PE with K-L formulation. Section IV revisits Broyden-based input SM and defines the stopping criteria used for the numerical comparisons presented in Section V. Finally, Section VI concludes our work.

II. Parameter Extraction Objective Functions

Numerical parameter extraction can be formulated as the following optimization problem:

$$\boldsymbol{x}^{\mathrm{PE}} = \arg \min_{\boldsymbol{x}} U_{\mathrm{PE}}\left(\boldsymbol{R}(\boldsymbol{x}), \boldsymbol{R}^{\mathrm{t}}\right) \tag{1}$$

where the n model parameters are in vector $\boldsymbol{x} \in \Re^n$, the r model responses are represented by a multidimensional vector function $\boldsymbol{R}(\boldsymbol{x})$: $\Re^n \rightarrow \Re^r$, and vector $\boldsymbol{R}^{\mathrm{t}} \in \Re^r$ contains the target response for PE. The difference between $\boldsymbol{R}(\boldsymbol{x})$ and $\boldsymbol{R}^{\mathrm{t}}$ is measured by a multidimensional scalar PE objective function U_{PE}: $\Re^n \rightarrow \Re^1$. The purpose of PE, hopefully achieved by solving (1), is to find the optimal model parameters $\boldsymbol{x}^{\mathrm{PE}} \in \Re^n$ that make the model response $\boldsymbol{R}(\boldsymbol{x})$ as close as possible to the target response $\boldsymbol{R}^{\mathrm{t}}$. In the SM context, $\boldsymbol{R}^{\mathrm{t}}$ is obtained from the fine model, while $\boldsymbol{R}(\boldsymbol{x})$ is obtained from the coarse model.

The PE objective function using an l-th norm is

$$U_{\mathrm{PE}}\left(\boldsymbol{R}(\boldsymbol{x}), \boldsymbol{R}^{\mathrm{t}}\right) = \left\|\boldsymbol{e}(\boldsymbol{x})\right\|_l \tag{2}$$

where $\boldsymbol{e}(\boldsymbol{x}) \in \Re^r$ is the error of the model response with respect to the target response, $\boldsymbol{e}(\boldsymbol{x}) = \boldsymbol{R}(\boldsymbol{x}) - \boldsymbol{R}^{\mathrm{t}}$. The classical norms employed in (2) are Manhattan (l = 1), Euclidean (l = 2), and Chebyshev ($l \rightarrow \infty$) [9], defined respectively as

$$U_{\mathrm{PE}}^{\mathrm{M}} = \sum\nolimits_{j=1}^{r} \left|e_j(\boldsymbol{x})\right| \tag{3}$$

$$U_{\mathrm{PE}}^{\mathrm{E}} = \sum\nolimits_{j=1}^{r} e_j^2(\boldsymbol{x}) \tag{4}$$

$$U_{\mathrm{PE}}^{\mathrm{C}} = \max_j \left\{\cdots \left|e_j(\boldsymbol{x})\right| \cdots\right\} \tag{5}$$

Following [16], the difference between two general systems, A and B, can be represented by relative entropy [18] according to Shannon information theory [19]. This difference measured by the Kullback-Leibler (K-L) distance [12] is given by

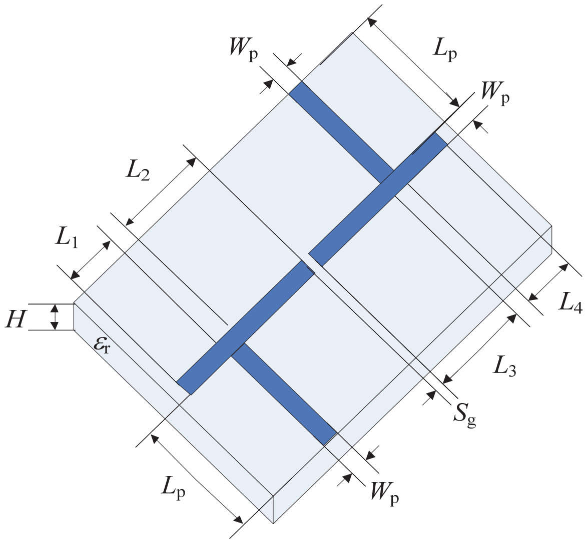

Fig. 3 Band-pass filter in microstrip technology [21]. The design parameters are $\boldsymbol{x} = [L_1 \;\; L_2 \;\; L_3 \;\; L_4 \;\; S_g]^T$. From [17].

$$C = \sum_{j=1}^{r} \left\{ A_j \ln \left| \frac{A_j}{B_j} \right| + (1 - A_j) \ln \left| \frac{1 - A_j}{1 - B_j} \right| \right\} \tag{6}$$

where C is the relative entropy between systems A and B, and A_j and B_j (j = 1, 2, … , r) are the j-th states of these systems. Adapting (6) to the PE objective function $U_{PE}(\boldsymbol{R}(\boldsymbol{x}),\boldsymbol{R}^t)$,

$$U_{PE}^{KL} = \sum_{j=1}^{r} \left\{ R_j(\boldsymbol{x}) \ln \left| \frac{R_j(\boldsymbol{x})}{R_j^t} \right| + \left(1 - R_j(\boldsymbol{x})\right) \ln \left| \frac{1 - R_j(\boldsymbol{x})}{1 - R_j^t} \right| \right\} \tag{7}$$

where R_j is the j-th model response at model parameters $\boldsymbol{x}$, and R_j^t is the j-th target response [16].

Since the PE objective function values using the above formulations significantly differ from each other, the following scaled PE objective function U_{PE}^s is used to make fair numerical comparisons and to apply the same termination criteria to stop the numerical optimization during PE,

$$U_{PE}^s = \frac{U_{PE}(\boldsymbol{x})}{U_{PE}(\boldsymbol{x}^{(0)})} \tag{8}$$

where $\boldsymbol{x}^{(0)} \in \Re^n$ is the starting point for numerical PE.

Considering that (6) has been employed to measure the difference between probabilistic distributions, then (7) could be useful to do PE not only for deterministic responses but also for model responses with statistical fluctuations. That potential property of K-L-based PE can be studied in a future contribution considering statistical manufacturing tolerances in the model parameters (beyond the scope of this paper).

III. PE Using l-th Norms and K-L

A low-pass and a band-pass microstrip filters are used in this section to compare the behavior of the PE sub-problem with classical l-th norm versus the K-L formulation.

A. PE Example 1: Low-Pass Microstrip Filter

As a first PE example we use the microstrip low-pass filter shown in Fig. 1 [20]. It has a substrate with a relative dielectric permittivity ε_r = 2.2, height H = 0.794 mm, and loss

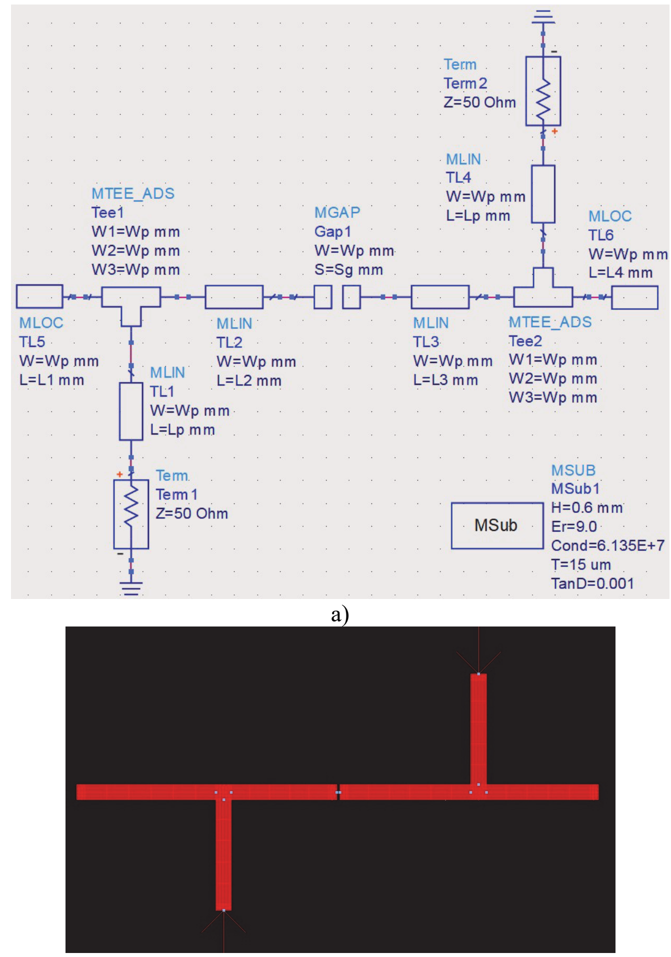

Fig. 4 Band-pass filter in microstrip technology: a) coarse model in ADS, b) fine model in ADS Momentum. From [17].

tangent tan(δ) = 0.01. Metal traces and ground plane use copper with thickness t = 15.24 μm and conductivity σ = 5.8×10^7 S/m. The input-output 50-Ω microstrip lines have a width W_p = 2.45 mm and a length L_p = 14H. They are separated by a distance S_1 with a microstrip line width W_1 and open stubs with length L_1. This filter has three design parameters $\boldsymbol{x} = [W_1 \;\; L_1 \;\; S_1]^T$. The pre-assigned parameters are $\boldsymbol{z} = [H \;\; \varepsilon_r \;\; W_p \;\; L_p \;\; \tan(\delta) \;\; \sigma \;\; t]^T$.

The coarse model is the Keysight ADS equivalent circuit shown in Fig. 2a. The full-wave EM fine model is in Keysight ADS Momentum Microwave, as shown in Fig. 2b, using a high-resolution discretization until EM resolution convergence is reached.

B. PE Example 2: Band-Pass Microstrip Filter

As a second PE example we use the microstrip band-pass filter shown in Fig. 3 [21]. The dielectric substrate uses alumina with ε_r = 9, H = 0.6 mm, and tan(δ) = 0.001. All microstrip lines used in this filter have the same width W_p = 0.7 mm. The feeding microstrip lines have a length L_p = 5 mm. Metallic strips and ground plane use t = 15 μm and σ = 5.8×10^7 S/m. Main resonators have lengths L_1, L_2, L_3, and L_4, with a separating gap S_g. This band-pass filter has five design parameters $\boldsymbol{x}$ = $[L_1 \;\; L_2 \;\; L_3 \;\; L_4 \;\; S_g]^T$ and seven pre-assigned

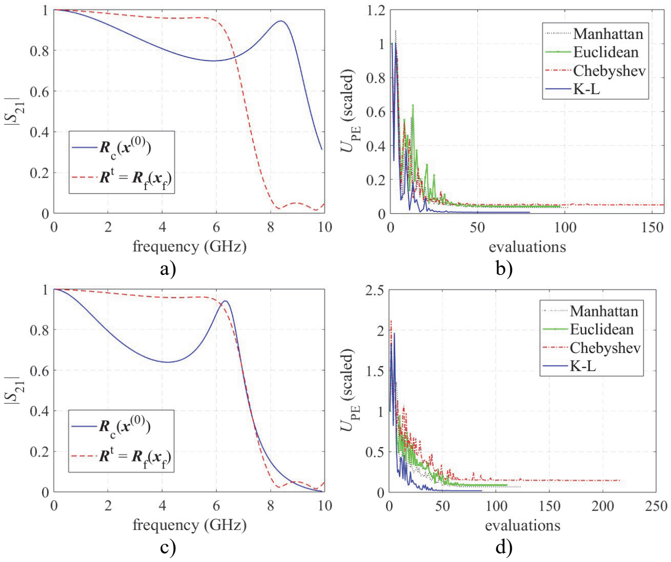

Fig. 5 PE results for the low-pass microstrip filter (see Fig. 1) using two different starting points $\boldsymbol{x}^{(0)}$ for the same target. a), c) EM response used as target $\boldsymbol{R}^{t}$ and initial coarse model response at the starting points, $\boldsymbol{R}_c(\boldsymbol{x}^{(0)})$; b), d) evolution of scaled U_{PE}. a) and b) use $\boldsymbol{x}^{(0)} = [4.0\ \ 3.0\ \ 2.0]^T$ mm (Case 1); c) and d) use $\boldsymbol{x}^{(0)} = [6.0\ \ 4.0\ \ 4.0]^T$ mm (Case 2). From [17].

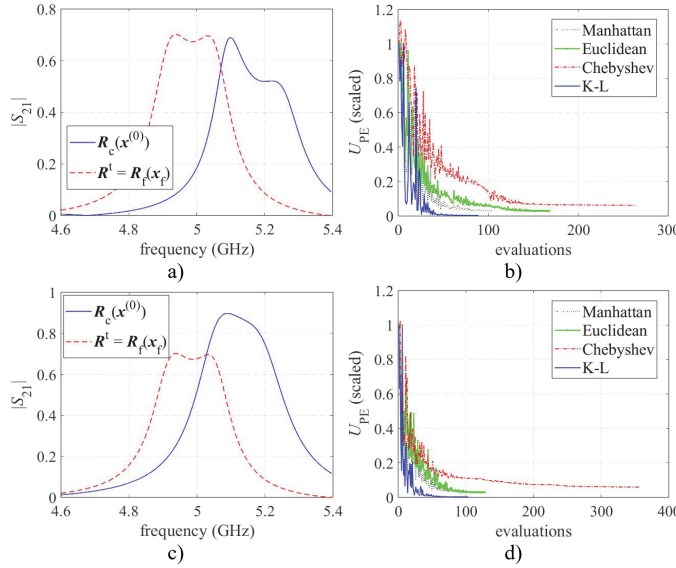

Fig. 6 PE results for the band-pass microstrip filter (see Fig. 3) using two different starting points $\boldsymbol{x}^{(0)}$ for the same target. a), c) EM filter response used as target $\boldsymbol{R}^{t}$ and initial coarse model response at the starting points, $\boldsymbol{R}_c(\boldsymbol{x}^{(0)})$; b), d) evolution of scaled U_{PE}. a) and b) use $\boldsymbol{x}^{(0)} = [6.2\ \ 4.6\ \ 5.9\ \ 5.1\ \ 0.15]^T$ mm (Case 1); c) and d) use $\boldsymbol{x}^{(0)} = [6.5\ \ 4.5\ \ 6.0\ \ 5.0\ \ 0.13]^T$ mm (Case 2). From [17].

parameters $\boldsymbol{z} = [H\ \ \varepsilon_r\ \ W_p\ \ \tan(\delta)\ \ \sigma\ \ t]^T$.

The coarse model is the Keysight ADS equivalent circuit shown in Fig. 4a. The corresponding full-wave EM fine model is in Keysight ADS Momentum Microwave, as shown in Fig. 4b, also using a fine resolution grid until resolution convergence is reached.

C. PE Results and Numerical Comparison

The following error metrics are used for numerical comparison between all the PE formulations: the average absolute relative error (ε_{avg}^{PE}), the maximum absolute relative error (ε_{max}^{PE}), and the normalized mean square error (ε_{nms}^{PE}), defined as

$$\varepsilon_{avg}^{PE} = \frac{100}{r} \frac{\| \boldsymbol{e}_{PE} \|_1}{\| \boldsymbol{R}^t \|_\infty}\ (\%) \tag{9}$$

$$\varepsilon_{max}^{PE} = 100 \frac{\| \boldsymbol{e}_{PE} \|_\infty}{\| \boldsymbol{R}^t \|_\infty}\ (\%) \tag{10}$$

$$\varepsilon_{nms}^{PE} = 100 \frac{\| \boldsymbol{e}_{PE} \|_2}{\| \boldsymbol{R}^t \|_2}\ (\%) \tag{11}$$

where $\boldsymbol{e}_{PE}$ is the error vector after PE, $\boldsymbol{e}_{PE} = \boldsymbol{R}(\boldsymbol{x}^{PE}) - \boldsymbol{R}^t$.

The target fine model response $\boldsymbol{R}^t$ for PE is obtained from the EM simulation at reference design $\boldsymbol{x}_f = [1.270\ \ 4.880\ \ 2.365]^T$ (mm) for the low-pass filter, and $\boldsymbol{x}_f = [6.275\ \ 4.75\ \ 5.90\ \ 5.05\ \ 0.15]^T$ (mm) for the band-pass filter. We consider two arbitrary starting points $\boldsymbol{x}^{(0)}$ for PE for each filter. The results are shown in Fig. 5 and Table I for the low-pass filter, and in Fig. 6 and Table II for the band-pass filter. In both examples we use the same optimization method (Nelder-Mead) with the same termination criteria for PE: tolerances employed for optimization variables (Δx) and objective function (ΔU_{PE}^{s}) are indicated in Tables I and II.

It is seen from Figs. 5 and 6 that, for both examples and both starting points, the K-L formulation requires less evaluations of the PE objective function than those needed by l-th norms, arriving to a smaller value of the scaled PE objective function. Tables I and II reconfirm those results and additionally indicate that K-L yields similar response matching errors than those obtained with l-th norms.

TABLE I. PE RESULTS FOR THE LOW-PASS FILTER USING THE NELDER-MEAD METHOD FOR EACH PE OBJECTIVE FUNCTION

$\boldsymbol{x}^{(0)}$	OF	i	$\boldsymbol{x}^{PE}$	ε_{avg}^{PE}	ε_{max}^{PE}	ε_{nms}^{PE}
Case 1	M	102	$[1.3729\ \ 5.3993\ \ 2.8353]^T$	0.93	5.40	2.10
	E	97	$[1.4973\ \ 5.3133\ \ 2.9794]^T$	1.02	4.94	2.01
	C	157	$[2.2123\ \ 4.9795\ \ 3.5190]^T$	0.41	4.64	3.65
	K-L	80	$[1.5159\ \ 5.2744\ \ 3.1133]^T$	1.06	4.95	2.06
Case 2	M	123	$[1.3722\ \ 5.3997\ \ 2.8358]^T$	0.93	5.41	2.10
	E	110	$[1.4984\ \ 5.3126\ \ 2.9799]^T$	1.03	4.94	2.01
	C	216	$[2.2177\ \ 4.9768\ \ 3.5229]^T$	0.41	4.64	3.67
	K-L	87	$[1.5157\ \ 5.2751\ \ 3.1106]^T$	1.06	4.95	2.06

OF is the PE objective function: Manhattan (M), Euclidean (E), Chebyshev (C), or Kullback-Leibler (K-L).
i is the total number of OF evaluations (or coarse model simulations) to get $\boldsymbol{x}^{PE}$.
Termination tolerances used for Nelder-Mead: $\Delta x = 1\times10^{-3}$ and $\Delta U_{PE}^{s} = 1\times10^{-3}$.

TABLE II. PE RESULTS FOR THE BAND-PASS FILTER USING THE NELDER-MEAD METHOD FOR EACH PE OBJECTIVE FUNCTION

$\boldsymbol{x}^{(0)}$	OF	i	$\boldsymbol{x}^{PE}$	ε_{avg}^{PE}	ε_{max}^{PE}	ε_{nms}^{PE}
Case 1	M	105	$[6.6199\ 4.7714\ 5.8767\ 5.3965\ 0.1338]^T$	1.23	4.27	3.06
	E	168	$[6.6440\ 4.7414\ 5.8708\ 5.4011\ 0.1300]^T$	1.24	2.58	2.77
	C	264	$[6.3725\ 4.9211\ 6.2208\ 5.2004\ 0.1386]^T$	0.16	5.49	6.82
	K-L	89	$[6.6094\ 4.7837\ 5.8934\ 5.3795\ 0.1380]^T$	1.56	7.92	4.57
Case 2	M	110	$[6.6489\ 4.7292\ 5.8664\ 5.4033\ 0.1237]^T$	1.32	2.8	2.86
	E	128	$[6.6553\ 4.7236\ 5.8654\ 5.4040\ 0.1242]^T$	1.32	2.43	2.83
	C	358	$[6.3755\ 4.9193\ 6.2568\ 5.1737\ 0.1375]^T$	0.14	5.94	7.63
	K-L	104	$[6.6215\ 4.7509\ 5.8855\ 5.3873\ 0.1246]^T$	1.53	6.11	4.31

OF and i are defined as in Table I.
Termination tolerances used for Nelder-Mead: $\Delta x = 1\times10^{-2}$ and $\Delta U_{PE}^{s} = 1\times10^{-4}$.

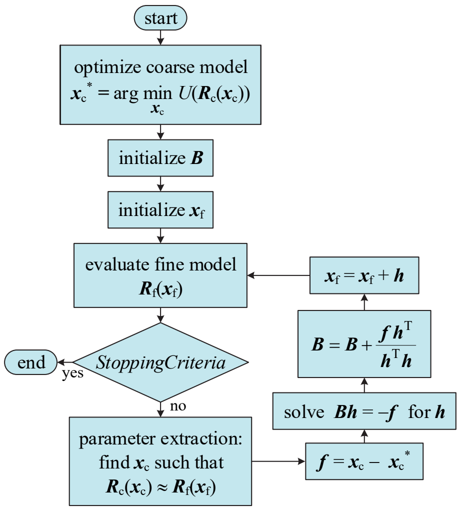

Fig. 7 Broyden-based input SM algorithm. From [7].

IV. Space Mapping (SM) Algorithm

The Broyden-based input SM algorithm, also known as aggressive space mapping (ASM), is shown in Fig. 7. First, the optimal coarse model design $\boldsymbol{x}_c^*$ is obtained [6] by finding the ideal response that optimally satisfies the design specifications, $\boldsymbol{R}_c(\boldsymbol{x}_c^*)$. Next, the Broyden matrix $\boldsymbol{B}$ is initialized, normally with the identity matrix [7]. Initially, the fine model response is evaluated at $\boldsymbol{x}_c^*$. If the stop criteria are not satisfied, then the PE sub-problem is solved to align the coarse model response $\boldsymbol{R}_c(\boldsymbol{x}_c)$ to the current fine model response $\boldsymbol{R}_f(\boldsymbol{x}_f)$. The difference $\boldsymbol{f}$ between the extracted parameters $\boldsymbol{x}_c$ and the optimal coarse model design $\boldsymbol{x}_c^*$ is calculated. Next, a quasi-Newton step $\boldsymbol{h}$ is calculated, $\boldsymbol{B}$ is updated using Broyden's formula, and the next iterate $\boldsymbol{x}_f$ is obtained where the new $\boldsymbol{R}_f(\boldsymbol{x}_f)$ is evaluated (see Fig. 7). This loop continues until the stopping criteria are satisfied, ending with a space-mapped solution $\boldsymbol{x}_f^{SM}$ [7].

For the PE sub-problem in ASM, here we solve (1) by using as target the fine model response at the i-th iteration, $\boldsymbol{R}_f(\boldsymbol{x}_f^{(i)})$, to extract the coarse model parameters $\boldsymbol{x}_c^{PE}$, that achieve the local alignment $\boldsymbol{R}_c(\boldsymbol{x}_c^{PE}) \approx \boldsymbol{R}_f(\boldsymbol{x}_f^{(i)})$. This is done by using the four PE objective functions described in Section II. Then, we compare the behavior of ASM obtained with classical norms (3)-(5) for PE versus that one obtained with the K-L formulation (7) used in the PE sub-problem.

The final goal of ASM is to find a space-mapped solution

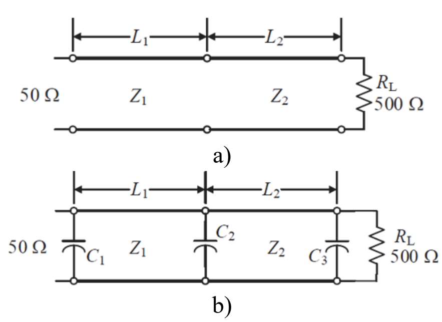

Fig. 8 Two-section impedance transformer: a) coarse model, b) fine model [16]. The design parameters are $\boldsymbol{x} = [L_1 \quad L_2]^T$.

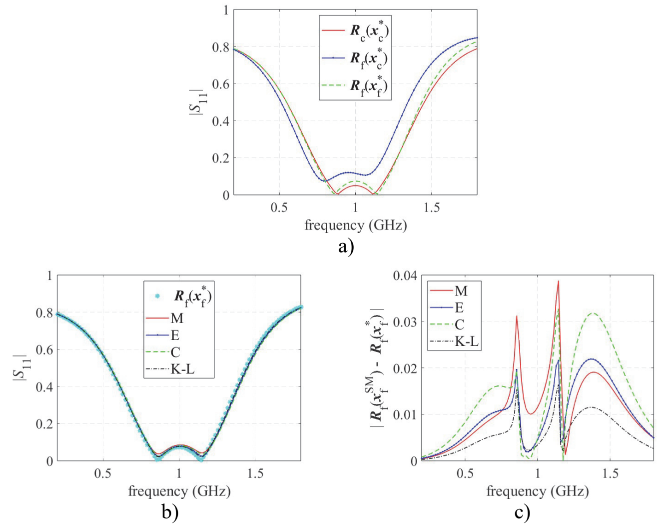

Fig. 9 SM results for the two-section impedance transformer. a) $\boldsymbol{R}_c(\boldsymbol{x}_c^*)$, $\boldsymbol{R}_f(\boldsymbol{x}_c^*)$, and $\boldsymbol{R}_f(\boldsymbol{x}_f^*)$; b) $\boldsymbol{R}_f(\boldsymbol{x}_f^{SM})$ using Manhattan (M), Euclidean (E), Chebyshev (C), and Kullback-Leibler (K-L) for PE, versus $\boldsymbol{R}_f(\boldsymbol{x}_f^*)$; c) corresponding matching error $|\boldsymbol{R}_f(\boldsymbol{x}_f^{SM}) - \boldsymbol{R}_f(\boldsymbol{x}_f^*)|$.

that makes the fine model response sufficiently close to the optimal coarse model response, $\boldsymbol{R}_f(\boldsymbol{x}_f^{SM}) \approx \boldsymbol{R}_c(\boldsymbol{x}_c^*)$.

Here, the stopping criteria (SC) used for ASM are [7]:

$$\left\| \boldsymbol{f}(\boldsymbol{x}_f^{(i)}) \right\|_\infty < \varepsilon_1 \ \vee \ \ldots \tag{12a}$$

$$\left\| \boldsymbol{R}_f(\boldsymbol{x}_f^{(i)}) - \boldsymbol{R}_c(\boldsymbol{x}_c^*) \right\|_\infty \le \varepsilon_2 (\varepsilon_2 + \left\| \boldsymbol{R}_c(\boldsymbol{x}_c^*) \right\|_\infty) \ \vee \ \ldots \tag{12b}$$

$$\left\| \boldsymbol{x}_f^{(i+1)} - \boldsymbol{x}_f^{(i)} \right\|_2 \le \varepsilon_3 (\varepsilon_3 + \left\| \boldsymbol{x}_f^{(i)} \right\|_2) \ \vee \ \ldots \tag{12c}$$

$$i > i_{max} \tag{12d}$$

where ε_1, ε_2 and ε_3 are arbitrary small positive scalars. Typically, i_{max} is $3n$ or $4n$ ($\boldsymbol{x}_f \in \Re^n$) [7].

V. SM Using L-th Norms and K-L for PE

The Broyden-based input SM algorithm with classical l-th norms and with the K-L distance for PE is implemented in this section and applied to several design optimization examples. The corresponding numerical results, including the $\boldsymbol{x}_f^{SM}$ found

Table III. SM Results for the Two-Section Impedance Transformer using Different Objective Functions for PE

OF	$\boldsymbol{x}_c^{(i)T}$	$\boldsymbol{x}_f^{(i)T}$	$N_c^{(i)}$	N_c^t	ε_{avg}^{SM}	ε_{max}^{SM}	ε_{nms}^{SM}	SC
M	[101.93 92.06] [91.34 88.25]	[90.00 90.00] [78.07 87.94] [76.60 89.85]	69 83	152	1.33	4.68	2.67	2
E	[102.10 92.51] [90.64 88.55]	[90.00 90.00] [77.90 87.49] [77.24 88.98]	65 71	136	1.20	2.65	2.37	2
C	[102.00 94.24] [88.54 89.66]	[90.00 90.00] [78.00 85.76] [79.31 86.06]	97 88	185	1.69	3.95	3.37	2
K-L	[102.19 92.41] [90.04 88.39]	[90.00 90.00] [77.81 87.59] [77.77 89.17]	64 68	132	0.68	1.98	1.35	2

OF is defined as in Table I.
$N_c^{(i)}$: number of coarse model evaluations per iteration.
N_c^t: total number of coarse model evaluations (considering all the iterations).
SC: stopping criteria satisfied for ending the space mapping algorithm.
Tolerances used for the SM algorithm: $\varepsilon_1 = 1\times10^{-1}$, $\varepsilon_2 = 1\times10^{-1}$ and $\varepsilon_3 = 1\times10^{-2}$.
Tolerances used for the PE sub-problem: $\Delta x = 1\times10^{-3}$ and $\Delta U_{PE}^s = 1\times10^{-3}$.

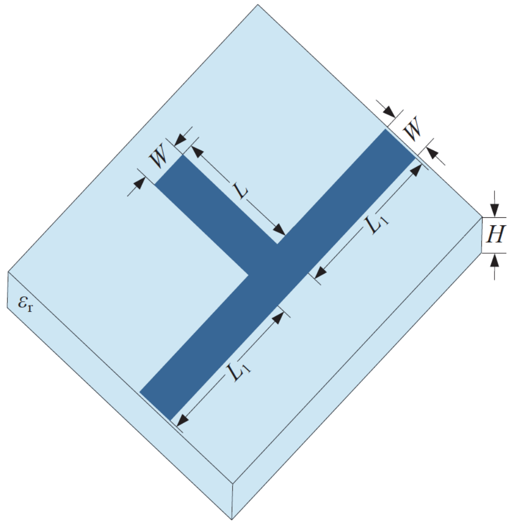

Fig. 10 Single-stub band-stop filter in microstrip technology [1]. The design parameter is $x = L$.

for each case, are rigorously compared. First, we apply SM to a classical synthetic test example (a two-section impedance transformer). Next, we apply it to three microstrip filters (band-stop, low-pass, and band-pass, respectively) whose fine models are accurate full-wave EM models, and their equivalent circuits are taken as coarse models.

A. SM Example 1: Classical Synthetic Test Example

As a first SM example, consider a classical synthetic test case: a capacitively-loaded 10:1 two-section impedance transformer. Ideal transmission lines are used in the coarse model, while capacitively-loaded transmission lines are used in the fine model, as shown in Fig. 8 [16].

The design parameters are $\boldsymbol{x} = [L_1 \;\; L_2]^T$ (degrees), with C_1 = 0.4 pF, C_2 = 0.2 pF and C_3 = 0.1 pF. The reference impedance for both models is Z_0 = 50 Ω and the load impedance is R_L = 500 Ω. The transmission lines characteristic impedances are kept fixed at $Z_1 = 1.8233Z_0$ Ω, and $Z_2 = 5.4845Z_0$ Ω, using coefficients for a Chebyshev profile with a 10:1 transformation ratio and a 0.05 ripple [22].

The optimal coarse model design (analytically obtained) is $\boldsymbol{x}_c^* = [90 \;\; 90]^T$ (degrees). The optimal fine model design (obtained from direct conventional optimization) is $\boldsymbol{x}_f^* = [79.0670 \;\; 88.6166]^T$. Responses are calculated from 0.2 to 1.8 GHz using p = 101 frequency points. The parameter extraction sub-problem considers the complete frequency range.

Fig. 9a shows the coarse model optimal response, $\boldsymbol{R}_c(\boldsymbol{x}_c^*)$, which is the target response for ASM, the fine model response at the optimal coarse model design, $\boldsymbol{R}_f(\boldsymbol{x}_c^*)$, which is the initial fine model response of the ASM algorithm, and the actual fine model optimal response, $\boldsymbol{R}_f(\boldsymbol{x}_f^*)$, which is normally unknown in a SM problem. Here we use $\boldsymbol{R}_f(\boldsymbol{x}_f^*)$ to assess the accuracy of the fine model response at the space-mapped solution $\boldsymbol{R}_f(\boldsymbol{x}_f^{SM})$

TABLE IV. SM RESULTS FOR THE BAND-STOP FILTER USING DIFFERENT OBJECTIVE FUNCTIONS FOR PE

OF	$\boldsymbol{x}_c^{(i)}$	$\boldsymbol{x}_f^{(i)}$	$N_c^{(i)}$	N_c^t	ε_{avg}^{SM}	ε_{max}^{SM}	ε_{nms}^{SM}	SC
M	6.4985 6.1850	6.1937 5.8889 5.8973	20 20	40	6.89×10^{-11}	8.57×10^{-11}	8.37×10^{-11}	1&3
E	6.5010 6.1848	6.1937 5.8864 5.8951	18 20	38	8.57×10^{-11}	1.06×10^{-10}	1.04×10^{-10}	1&3
C	6.5045 6.1899	6.1937 5.8829 5.8867	28 34	62	1.52×10^{-10}	1.88×10^{-10}	1.85×10^{-10}	1&3
K-L	6.4889 6.1906	6.1937 5.8985 5.9016	16 20	36	3.48×10^{-11}	4.37×10^{-11}	4.23×10^{-11}	1&3

OF is defined as in Table I. $N_c^{(i)}$, N_c^t and SC are defined as in Table III.
Tolerances used for the SM algorithm: $\varepsilon_1 = 1\times10^{-2}$, $\varepsilon_2 = 1\times10^{-2}$ and $\varepsilon_3 = 1\times10^{-2}$.
Tolerances used for the PE sub-problem: $\Delta x = 1\times10^{-2}$ and $\Delta U_{PE}^{s} = 1\times10^{-5}$.

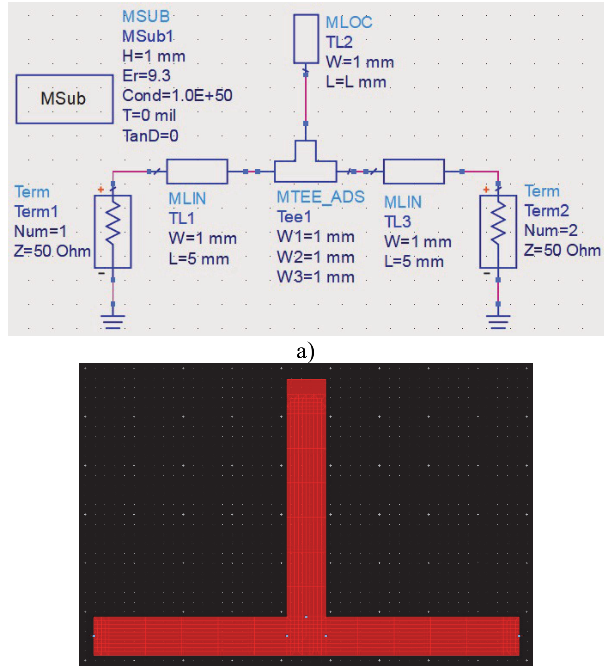

Fig. 11 Single-stub band-stop filter in microstrip technology: a) coarse model in ADS, b) fine model in ADS Momentum.

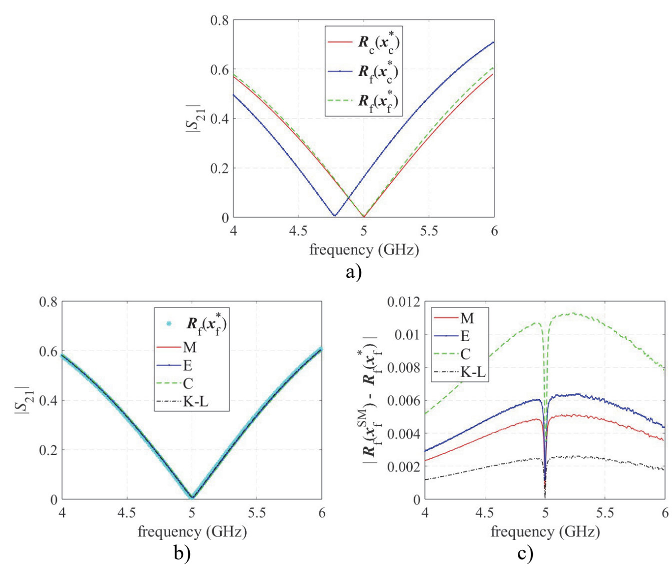

Fig. 12 SM results for the single-stub band-stop microstrip filter (see Fig. 10). a) $\boldsymbol{R}_c(\boldsymbol{x}_c^*)$, $\boldsymbol{R}_f(\boldsymbol{x}_c^*)$, and $\boldsymbol{R}_f(\boldsymbol{x}_f^*)$; b) $\boldsymbol{R}_f(\boldsymbol{x}_f^{SM})$ using Manhattan (M), Euclidean (E), Chebyshev (C), and Kullback-Leibler (K-L) for PE, versus $\boldsymbol{R}_f(\boldsymbol{x}_f^*)$; c) corresponding matching error $|\boldsymbol{R}_f(\boldsymbol{x}_f^{SM})–\boldsymbol{R}_f(\boldsymbol{x}_f^*)|$.

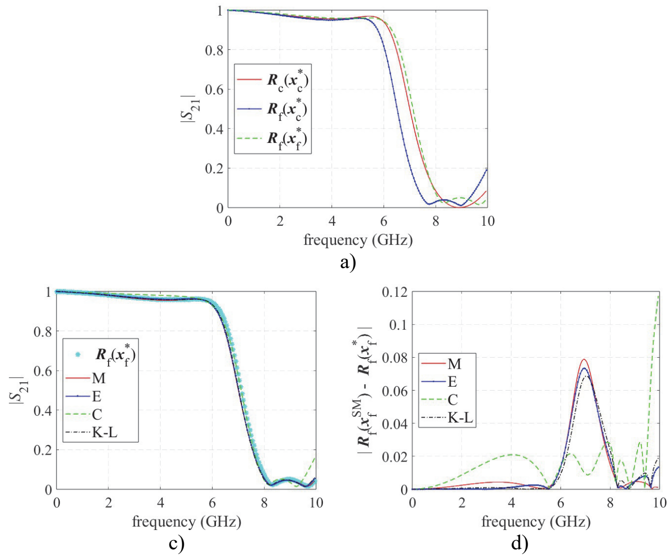

Fig. 13 SM results for the low-pass microstrip filter (see Fig. 1). a) $\boldsymbol{R}_c(\boldsymbol{x}_c^*)$, $\boldsymbol{R}_f(\boldsymbol{x}_c^*)$, and $\boldsymbol{R}_f(\boldsymbol{x}_f^*)$; b) $\boldsymbol{R}_f(\boldsymbol{x}_f^{SM})$ using Manhattan (M), Euclidean (E), Chebyshev (C), and Kullback-Leibler (K-L) for PE, versus $\boldsymbol{R}_f(\boldsymbol{x}_f^*)$; c) corresponding matching error $|\boldsymbol{R}_f(\boldsymbol{x}_f^{SM})$-$\boldsymbol{R}_f(\boldsymbol{x}_f^*)|$.

obtained when using the ASM algorithm with classical l-th norms and the K-L formulation. The same is done in the following examples.

B. SM Example 2: Single-Stub Band-Stop Microstrip Filter

As a second SM example, consider the single-stub band-stop microstrip filter reported in [1] and illustrated in Fig. 10. The coarse model uses a Keysight ADS equivalent circuit (see Fig. 11a). The fine model uses full-wave EM simulations in Keysight ADS Momentum Microwave with a high-resolution discretization until convergence is reached (see Fig. 11b).

This band-stop microstrip filter has only one design parameter $x = L$ (mm). The pre-assigned parameters are $\boldsymbol{z} = [H \quad \varepsilon_r \quad W \quad L_1]^T$, with a substrate thickness H = 1 mm, relative dielectric permittivity ε_r = 9.3, microstrips width W = 1 mm, and input/output microstrips length L_1 = 5 mm. These values of H, ε_r, and W yield a characteristic impedance $Z_0 \approx 50\ \Omega$. In this example, losses are neglected and metals are considered as infinitesimally thin conductors, *i.e.*, loss tangent $\tan(\delta) = 0$, metal thickness $t = 0$, and conductivity σ is infinite.

The optimal fine model design is $\boldsymbol{x}_f^*$ = 5.906 and the optimal coarse model design is $\boldsymbol{x}_c^*$ = 6.1937. Fig. 12a shows $\boldsymbol{R}_c(\boldsymbol{x}_c^*)$, $\boldsymbol{R}_f(\boldsymbol{x}_c^*)$ and $\boldsymbol{R}_f(\boldsymbol{x}_f^*)$.

TABLE V. SM RESULTS FOR THE LOW-PASS FILTER USING DIFFERENT OBJECTIVE FUNCTIONS FOR PE

OF	$\boldsymbol{x}_c^{(i)T}$	$\boldsymbol{x}_f^{(i)T}$	$N_c^{(i)}$	N_c^t	ε_{avg}^{SM}	ε_{max}^{SM}	ε_{nms}^{SM}	SC
	[1.71 5.60 3.74]	[1.52 5.27 3.11]	73					
M	[1.39 5.41 2.83]	[1.32 4.95 2.49]	91	164	1.21×10^{-10}	7.93×10^{-10}	4.20×10^{-10}	3
		[1.41 4.85 2.70]						
	[1.79 5.60 3.72]	[1.52 5.27 3.11]	70					
E	[1.45 5.32 3.01]	[1.24 4.95 2.51]	61	131	1.14×10^{-10}	7.38×10^{-10}	4.02×10^{-10}	3
		[1.30 4.92 2.60]						
	[2.24 5.42 4.02]	[1.52 5.27 3.11]	151					
C	[1.62 5.09 3.33]	[0.79 5.13 2.21]	119	270	1.61×10^{-10}	1.18×10^{-09}	4.14×10^{-10}	3
		[0.66 5.35 1.94]						
	[1.76 5.59 3.79]	[1.52 5.27 3.11]	65					
K-L	[1.49 5.29 3.06]	[1.28 4.96 2.44]	45	110	1.10×10^{-10}	6.90×10^{-10}	3.84×10^{-10}	1&3
		[1.30 4.94 2.49]						

OF is defined as in Table I. $N_c^{(i)}$, N_c^t and SC are defined as in Table III.
Tolerances used for the SM algorithm: $\varepsilon_1 = 1\times10^{-1}$, $\varepsilon_2 = 1\times10^{-2}$ and $\varepsilon_3 = 1\times10^{-1}$.
Tolerances used for the PE sub-problem: $\Delta x = 1\times10^{-2}$ and $\Delta U_{PE}^{s} = 1\times10^{-5}$.

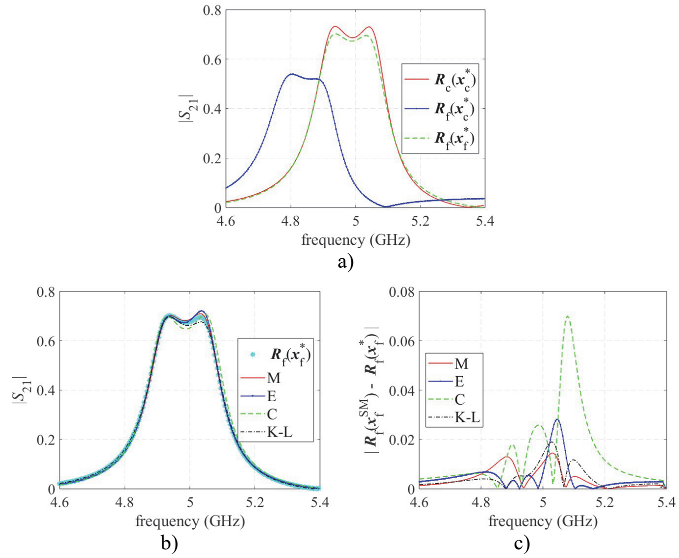

Fig. 14 SM results for the band-pass microstrip filter (see Fig. 3) using the Nelder-Mead optimization method for PE at each SM iteration. a) $\boldsymbol{R}_c(\boldsymbol{x}_c^*)$, $\boldsymbol{R}_f(\boldsymbol{x}_c^*)$, and $\boldsymbol{R}_f(\boldsymbol{x}_f^*)$; b) $\boldsymbol{R}_f(\boldsymbol{x}_f^{SM})$ using Manhattan (M), Euclidean (E), Chebyshev (C), and Kullback-Leibler (K-L) for PE, versus $\boldsymbol{R}_f(\boldsymbol{x}_f^*)$; c) corresponding matching error $|\boldsymbol{R}_f(\boldsymbol{x}_f^{SM}) - \boldsymbol{R}_f(\boldsymbol{x}_f^*)|$.

C. SM Example 3: Low-Pass Microstrip Filter

As a third SM example, consider the low-pass microstrip filter described in Section III.A. The optimal fine model design is $\boldsymbol{x}_f^* = [1.270 \quad 4.880 \quad 2.365]^T$ and the optimal coarse model design is $\boldsymbol{x}_c^* = [1.5159 \quad 5.2744 \quad 3.1133]^T$. $\boldsymbol{R}_c(\boldsymbol{x}_c^*)$, $\boldsymbol{R}_f(\boldsymbol{x}_c^*)$ and $\boldsymbol{R}_f(\boldsymbol{x}_f^*)$ are shown in Fig. 13a.

D. SM Example 4: Band-Pass Microstrip Filter

As the final SM example, consider the band-pass filter described in Section III.B. The optimal fine model design is $\boldsymbol{x}_f^* = [6.275 \quad 4.75 \quad 5.9 \quad 5.05 \quad 0.15]^T$ and the optimal coarse model design is $\boldsymbol{x}_c^* = [6.6094 \quad 4.7837 \quad 5.8934 \quad 5.3795$

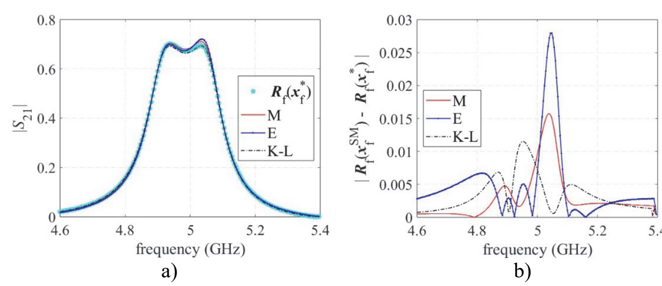

Fig. 15 SM results results for the band-pass microstrip filter (see Fig. 3) when the gradient-based constrained interior-point optimization method is used for PE at each SM iteration (instead of Nelder-Mead). $\boldsymbol{R}_c(\boldsymbol{x}_c^*)$, $\boldsymbol{R}_f(\boldsymbol{x}_c^*)$, and $\boldsymbol{R}_f(\boldsymbol{x}_f^*)$ are the same as those in Fig. 14a. a) $\boldsymbol{R}_f(\boldsymbol{x}_f^{SM})$ using Manhattan (M), Euclidean (E), and Kullback-Leibler (K-L) for PE, versus $\boldsymbol{R}_f(\boldsymbol{x}_f^*)$; c) corresponding matching error $|\boldsymbol{R}_f(\boldsymbol{x}_f^{SM}) - \boldsymbol{R}_f(\boldsymbol{x}_f^*)|$. In this case, the Chebyshev norm for PE makes SM to diverge (see Table VII).

TABLE VI. SM RESULTS FOR THE BAND-PASS FILTER USING DIFFERENT OBJECTIVE FUNCTIONS FOR PE AND THE NELDER-MEAD OPTIMIZATION METHOD FOR PE

OF	$\boldsymbol{x}_c^{(i)}$	$\boldsymbol{x}_f^{(i)}$	$N_c^{(i)}$	N_c^t	ε_{avg}^{SM}	ε_{max}^{SM}	ε_{nms}^{SM}	SC
	$[6.92\ \ 4.86\ \ 5.94\ \ 5.68\ \ 0.13]^T$	$[6.61\ \ 4.78\ \ 5.89\ \ 5.38\ \ 0.14]^T$	165					
M	$[6.64\ \ 4.73\ \ 5.84\ \ 5.42\ \ 0.12]^T$	$[6.30\ \ 4.71\ \ 5.85\ \ 5.08\ \ 0.14]^T$	289	454	8.03×10^{-11}	2.70×10^{-10}	1.18×10^{-10}	1&3
		$[6.26\ \ 4.77\ \ 5.91\ \ 5.04\ \ 0.16]^T$						
	$[6.94\ \ 4.82\ \ 5.92\ \ 5.69\ \ 0.11]^T$	$[6.61\ \ 4.78\ \ 5.89\ \ 5.38\ \ 0.14]^T$	293					
E	$[6.65\ \ 4.74\ \ 5.85\ \ 5.42\ \ 0.14]^T$	$[6.28\ \ 4.75\ \ 5.87\ \ 5.07\ \ 0.16]^T$	289	582	9.09×10^{-11}	5.22×10^{-10}	1.50×10^{-10}	1&3
		$[6.24\ \ 4.80\ \ 5.92\ \ 5.03\ \ 0.16]^T$						
	$[6.48\ \ 5.14\ \ 6.37\ \ 5.47\ \ 0.12]^T$	$[6.61\ \ 4.78\ \ 5.89\ \ 5.38\ \ 0.14]^T$	360					
C	$[6.96\ \ 4.53\ \ 5.47\ \ 5.57\ \ 0.15]^T$	$[6.74\ \ 4.43\ \ 5.41\ \ 5.29\ \ 0.15]^T$	298	856	2.56×10^{-10}	1.30×10^{-09}	4.16×10^{-10}	3
	$[6.83\ \ 4.62\ \ 5.68\ \ 5.49\ \ 0.14]^T$	$[6.55\ \ 4.56\ \ 5.64\ \ 5.18\ \ 0.15]^T$	198					
		$[6.22\ \ 4.81\ \ 5.90\ \ 5.03\ \ 0.14]^T$						
	$[6.89\ \ 4.89\ \ 5.94\ \ 5.68\ \ 0.13]^T$	$[6.61\ \ 4.78\ \ 5.89\ \ 5.38\ \ 0.14]^T$	101					
K-L	$[6.64\ \ 4.74\ \ 5.86\ \ 5.40\ \ 0.14]^T$	$[6.33\ \ 4.68\ \ 5.85\ \ 5.08\ \ 0.14]^T$	160	261	8.32×10^{-11}	3.52×10^{-10}	1.25×10^{-10}	1&3
		$[6.29\ \ 4.72\ \ 5.88\ \ 5.06\ \ 0.14]^T$						

OF is defined as in Table I. $N_c^{(i)}$, N_c^t and SC are defined as in Table III.
Tolerances used for the SM algorithm: $\varepsilon_1 = 2.5\times10^{-1}$, $\varepsilon_2 = 1\times10^{-1}$ and $\varepsilon_3 = 1\times10^{-2}$.
Tolerances used for the PE sub-problem: $\Delta x = 1\times10^{-2}$ and $\Delta U_{PE}^s = 1\times10^{-5}$.

$0.1380]^T$. Fig. 14a shows $\boldsymbol{R}_c(\boldsymbol{x}_c^*)$, $\boldsymbol{R}_f(\boldsymbol{x}_c^*)$ and $\boldsymbol{R}_f(\boldsymbol{x}_f^*)$.

E. SM Results and Comparison

The following error metrics are used for numerical comparisons to assess the fine model response at the space-mapped solution $\boldsymbol{R}_f(\boldsymbol{x}_f^{SM})$ found by ASM using all the PE formulations: the average absolute relative error (ε_{avg}^{SM}), the maximum absolute relative error (ε_{max}^{SM}), and the normalized mean square error (ε_{nms}^{SM}), defined as

$$\varepsilon_{avg}^{SM} = \frac{100}{r}\frac{\|\boldsymbol{e}_{SM}\|_1}{\|\boldsymbol{R}_f(\boldsymbol{x}_f^*)\|_\infty}\ (\%) \tag{13}$$

$$\varepsilon_{max}^{SM} = 100\frac{\|\boldsymbol{e}_{SM}\|_\infty}{\|\boldsymbol{R}_f(\boldsymbol{x}_f^*)\|_\infty}\ (\%) \tag{14}$$

$$\varepsilon_{nms}^{SM} = 100\frac{\|\boldsymbol{e}_{SM}\|_2}{\|\boldsymbol{R}_f(\boldsymbol{x}_f^*)\|_2}\ (\%) \tag{15}$$

where $\boldsymbol{e}_{SM} = \boldsymbol{R}_f(\boldsymbol{x}_f^{SM}) - \boldsymbol{R}_f(\boldsymbol{x}_f^*)$.

The SM results are shown in Fig. 9 and Table III for the synthetic test example, in Fig. 12 and Table IV for the single-stub band-stop microstrip filter, in Fig. 13 and Table V for the low-pass microstrip filter, and finally in Fig. 14 and Table VI for the band-pass microstrip filter.

In all these examples we use the same optimization method (Nelder-Mead) for PE with the same termination criteria. Tolerances for the PE sub-problem and for SM are indicated in Tables III-VI. The exiting stop criteria (SC) are represented in Tables III-VI by numbers 1 through 4, which correspond to those in (12), respectively.

We can see from Tables III-VI that the Broyden-based input SM algorithm with the K-L formulation used for the PE sub-problem outperforms that one with classical norms for PE given the following attributes: 1) it yields similar errors (13)-(15) in the final fine model response found; 2) it ends with similar or better stopping criteria (SC) satisfied; 3) it takes equal or less fine model evaluations to obtain the SM solution; and 4) it requires less or much less evaluations of the coarse model in the whole SM optimization cycle. These results are consistent with our findings in [16], where the K-L formulation produces smoother PE objective functions with larger dynamic ranges as compared to those produced with classical l-th norms.

By contrasting the overall results in Tables III-VI, it is also observed that, as we increase the complexity and the dimensionality of the problem, the K-L formulation for PE makes SM exhibit a clearer enhanced performance as compared to that one using classical norms for PE.

It is well known that the overall CPU time employed by any SM technique essentially depends on the number of fine

TABLE VII. SM RESULTS FOR THE BAND-PASS FILTER USING DIFFERENT OBJECTIVE FUNCTIONS FOR PE AND THE GRADIENT-BASED CONSTRAINED INTERIOR-POINT OPTIMIZATION METHOD FOR PE

OF	$\boldsymbol{x}_c^{(i)}$	$\boldsymbol{x}_f^{(i)}$	$N_c^{(i)}$	N_c^t	ε_{avg}^{SM}	ε_{max}^{SM}	ε_{nms}^{SM}	SC
	[6.92 4.84 5.93 5.68 1.22]	[6.61 4.78 5.89 5.38 0.14]	383					
M	[6.64 4.75 5.85 5.41 0.14]	[6.30 4.73 5.86 5.07 0.15]	209	592	5.53×10^{-11}	9.34×10^{-11}	2.92×10^{-10}	3
		[6.27 4.77 5.91 5.04 0.15]						
	[6.94 4.82 5.92 5.69 0.11]	[6.61 4.78 5.89 5.38 0.14]	217					
E	[6.65 4.74 5.85 5.42 1.41]	[6.28 4.75 5.87 5.07 0.16]	178	395	8.95×10^{-11}	1.48×10^{-10}	5.18×10^{-10}	1&3
		[6.24 4.80 5.92 5.03 0.16]						
	[0.11 0.13 6.00 5.67 1.00]	[6.61 4.78 5.89 5.38 0.14]	338					
C	[6.24 5.85 5.92 5.33 0.10]	[13.11 9.43 5.79 5.09 0.18]	139	NA	NA	NA	NA	NA
	[6.18 5.77 6.00 5.27 0.13]	[13.46 8.41 5.76 5.13 0.21]	66					
	[NA NA NA NA NA]	[27.63 **-24.16** 2.20 8.86 0.32]						
	[6.91 4.85 5.93 5.68 0.12]	[6.61 4.78 5.89 5.38 0.14]	145					
K-L	[6.63 4.75 5.86 5.40 0.14]	[6.31 4.72 5.85 5.08 0.15]	132	277	6.36×10^{-11}	8.71×10^{-11}	2.14×10^{-10}	3
		[6.28 4.75 5.89 5.06 0.15]						

OF is defined as in Table I. $N_c^{(i)}$, N_c^t and SC are defined as in Table III.
Tolerances used for the SM algorithm: $\varepsilon_1 = 2.5\times10^{-1}$, $\varepsilon_2 = 1\times10^{-1}$ and $\varepsilon_3 = 1\times10^{-2}$.
Tolerances used for the PE sub-problem: $\Delta x = 1\times10^{-5}$ and $\Delta U_{PE}^s = 1\times10^{-5}$.

model evaluations. However, if the coarse model in a given SM problem is not that computationally inexpensive, performing less coarse model evaluations during PE at each SM iteration can also produce a non-negligible speed up. For instance, in the fourth SM example (see Table VI), the total execution time (minutes:seconds) of all the coarse model evaluations for PE is 05:38 by K-L formulation, 09:48 by Manhattan norm, 12:33 by Euclidean norm, and 18:27 by Chebyshev norm, using a conventional laptop computer (AMD Ryzen® 7 5700U processor with AMD Radeon® Graphics 1.80 GHz and 16 GB RAM).

Regarding the numerical optimization method employed for PE, in [16] we use not only the Nelder-Mead method to compare PE with a K-L formulation versus classical norms, but also the trust region interior-reflective Newton method, which is a gradient-based method, as well as a comparison based on the graphical contours of the corresponding PE objective functions, making our conclusions on PE behavior independent of the optimization technique employed for PE [16]. To study the effects of changing the optimization method for PE in SM, we solved again the fourth example by using the gradient-based constrained interior-point optimization method available in Matlab to perform PE at each SM iteration. The corresponding results are shown in Table VII and Fig. 15. It is seen that these results fully support our previous conclusions, confirming the benefits of using a K-L formulation against using classical norms for PE in classical Broyden-based input SM. It is also seen in Table VII that SM fails (diverges) when using a Chebyshev norm for PE and the gradient-based constrained interior-point optimization method to do PE at each SM iteration.

Finally, the proposed new formulation for Broyden-based input SM using a K-L distance for PE can also be applied to design optimization problems in other microwave technologies, such as waveguide technology. Several problems in waveguide and other technologies might be considered in a future and more general contribution.

VI. Conclusion

A Broyden-based input space mapping (SM) algorithm, using a Kullback-Leibler (K-L) formulation as objective function for the parameter extraction (PE) sub-problem, was proposed for the first time. First, we applied PE with the K-L formulation to microstrip filters using their full-wave electromagnetic (EM) responses as targets, and we performed a rigorous numerical comparison against PE with classical norms. Next, we applied SM design optimization, using PE with the K-L formulation, to several examples, beginning with a classical synthetic example and following with some microstrip filters whose full-wave EM simulations were used as fine models, and their equivalent distributed circuits were used as coarse models. Then, we performed a rigorous numerical comparison between classical l-th norms and the K-L formulation for PE within the corresponding SM design optimizations. Our results indicate that Broyden-based input SM with the K-L formulation in the PE sub-problem outperforms that one with classical l-th norms. Other SM techniques that require performing PE could similarly benefit from the K-L formulation.

References

[1] S. Koziel, Q. S. Cheng, and J. W. Bandler, "Space mapping," *IEEE Microw. Mag.*, vol. 9, no. 6, pp. 105-122, Dec. 2008.

[2] Q. S. Cheng, J. W. Bandler and S. Koziel, "Combining coarse and fine models for optimal design," in *IEEE Microwave Mag.*, vol. 9, no. 1, pp. 79-88, Feb. 2008.

[3] J. E. Rayas-Sánchez, S. Koziel, and J. W. Bandler, "Advanced RF and microwave design optimization: a journey and a vision of future trends," *IEEE J. of Microwaves*, vol. 1, no. 1, pp. 481-493, Jan. 2021.

[4] J. W. Bandler, Q. Cheng, S. A. Dakroury, A. S. Mohamed, M. H. Bakr, K. Madsen, and J. Søndergaard, "Space mapping: the state of the art," *EEE Trans. Microw. Theory Tech.*, vol. 52, no. 1, pp. 337-361, Jan. 2004.

[5] J. E. Rayas-Sánchez, Q. J. Zhang, J. W. Rautio, N. K. Nikolova, V. E. Boria, Q. S. Cheng, M. Yu, and W. J. R. Hoefer, "Microwave modeling and design optimization: The legacy of John Bandler," *IEEE Trans. Microwave Theory Techn.*, vol. 73, no. 01, pp. 87-101, Jan. 2025.

[6] J. W. Bandler, R. M. Biernacki, S. H. Chen, R. H. Hemmers, and K. Madsen, "Electromagnetic optimization exploiting aggressive space mapping," *IEEE Trans. Microw. Theory Tech*., vol. 41, no. 12, pp. 2874-2882, Dec. 1995.

[7] J. E. Rayas-Sánchez, "Power in simplicity with ASM: tracing the aggressive space mapping algorithm over two decades of development and engineering applications," *IEEE Microw. Mag*., vol. 17, no. 4, pp. 64-76, Apr. 2016.

[8] J. W. Bandler, R. M. Biernacki, S. H. Chen, and D. Omeragić, "Space mapping optimization of waveguide filters using finite element and mode-matching electromagnetic simulators," *Int. J. RF Microw. Computer-Aided Eng*., vol. 9, no. 1, pp. 54-70, Jan. 1999.

[9] J. W. Bandler and J. E. Rayas-Sánchez, "An early history of optimization technology for automated design of microwave circuits," *IEEE J. Microwaves*, vol. 3, no. 1, pp. 319-337, Jan. 2023.

[10] J. E. Rayas-Sánchez, "Cognitive parameter extraction for space mapping design optimization," in *IEEE MTT-S Latin America Microwave Conf. (LAMC-2025)*, San Juan, Puerto Rico, Jan. 2025, pp. 9-12.

[11] J. E. Rayas-Sánchez, "Cognitive Broyden-based input space mapping for design optimization," *IEEE Microwave Wireless Tech. Lett.*, vol. 35, no. 6, pp. 760-763, Jun. 2025.

[12] S. Kullback and R. Leibler, "On the information and sufficiency", *Ann. Math. Statist.,* vol. 22, pp. 79-86, 1951.

[13] R. Veldhuis and E. Klabbers, "On the computation of the Kullback-Leibler measure for spectral distances", *IEEE Trans. Speech Audio Processing*, vol. 11, no. 1, pp. 100-103, Jan. 2003.

[14] N. Do and M. Vetterli, "Wavelet-based texture retrieval using generalized Gaussian density and Kullback-Leibler", *IEEE Tran. Image Processing*, vol. 11, no. 2, pp. 146-158, Feb. 2002.

[15] A. Vergara, M. Muezzinoglu, N. Rulkov, and E. Huerta, "Kullback-Leibler distance optimization for artificial chemo-sensors", in *IEEE Sensors Conf.*, La Jolla, CA, Nov. 2009, pp. 1146-1150.

[16] R. Loera-Díaz and J. E. Rayas-Sánchez, "An objective function formulation for circuit parameter extraction based on the Kullback-Leibler distance," in *IEEE MTT-S Int. Microw. Symp. Dig.*, Los Angeles, CA, Aug. 2020, pp. 80-82.

[17] R. Loera-Díaz, J. E. Rayas-Sánchez, and E. R. Villa-Loustaunau, "A rigorous numerical comparison for parameter extraction using classical and Kullback-Leibler formulations illustrated with full-wave EM and equivalent circuit models for microstrip filters," in *IEEE MTT-S Latin America Microw. Conf. (LAMC)*, San Juan, PR, USA, Jan. 2025, pp. 93-96.

[18] Y. Zhao, G. Xi, and J. Yi, "BP algorithm based on cross entropy function criterion", *Jisuanji Gongcheng/Computer Engineering*, vol. 31, no. 19, pp. 12-14, Oct. 2005.

[19] R. J. McEliece, *The Theory of Information and Coding*, New York, NY: Cambridge Univ. Press, 2001.

[20] D. M. Sheen, S. M. Ali, M. D. Abouzahra, and J. A. Kong, "Application of the three-dimensional finite-difference time-domain method to the analysis of planar microstrip circuits," *IEEE Trans. Microw. Theory Tech*., vol. 38, no. 7, pp. 849-857, July 1990.

[21] A. Hennings, E. Semouchkina, A. Baker, and G. Semouchkin, "Design optimization of bandpass filters with normally fed microstrip resonators

loaded by high-permittivity dielectric," *IEEE Trans. Microw. Theory Tech*., vol. 54, no. 3, pp. 1253-1261, Mar. 2006.
[22] D. M. Pozar, *Microwave Engineering*. Hoboken, NJ: John Wiley & Sons, Inc., 2005.

Roberto Loera-Díaz received the B.Sc. degree in communications and electronics from the University of Guadalajara, Mexico, in 2007 and the M.Sc. degree in electrical engineering from the Advanced Studies and Research Center, National Polytechnic Institute (CINVESTAV-IPN), Guadalajara, Mexico, in 2011.

He is currently working toward the Ph.D. degree in engineering sciences with the Department of Electronics, Systems, and Informatics, ITESO–The Jesuit University of Guadalajara.

Since 2012, he is an electrical engineer with Continental AG. His current research interests include numerical optimization methods for high frequency circuits, signal integrity, design of experiments, and surrogate-based optimization.

José E. Rayas-Sánchez (IEEE S'88-M'89-SM'95) received the B.Sc. degree in electronics engineering from ITESO, Guadalajara, Mexico, in 1984, the M.Sc. degree in electrical engineering from ITESM, Monterrey, Mexico, in 1989, and the Ph.D. degree in electrical engineering from McMaster University, Hamilton, Ontario, Canada, in 2001.

He is *Profesor Numerario* (hons.) and Emeritus Professor with ITESO–The Jesuit University of Guadalajara, where he leads the Research Group on Computer-Aided Engineering of Circuits and Systems (CAECAS). He is a member of the Mexican National System of Researchers (SNII), Level III. His research focuses on computer-aided and knowledge-based modeling and design optimization of high-frequency circuits.

Since 2019, Dr. Rayas-Sánchez is the IEEE Microwave Theory and Technology Society (MTT-S) Representative for the IEEE EDA Council (CEDA). Since 2024, he is an Associate Editor of the IEEE Microwave and Wireless Technology Letters. Since 2013, he is the IEEE MTT-S Regional Coordinator for Latin America. He was the General Chair of the First IEEE MTT-S Int. Microwave Workshop Series in Region 9 (IMWS2009-R9) on Signal Integrity and High-Speed Interconnects (Guadalajara, Mexico, Feb. 2009), as well as the General Chair of the First IEEE MTT-S Latin America Microwave Conference (LAMC-2016, Puerto Vallarta, Mexico, Dec. 2016). He was an elected AdCom member of the IEEE MTT-S for the years 2016-2024.